Journal of Power Sources 223 (2013) 36–41

Contents lists available at SciVerse ScienceDirect

Journal of Power Sources

journal homepage: www.elsevier.com/locate/jpowsour

Short communication

Preparation of dense silicate electrolyte coating with low pressure plasma spraying and very low pressure plasma spraying for intermediate-temperature solid oxide fuel cells

Fu Sun [a,b,*], Nannan Zhang [b], Jinglong Li [a], Hanlin Liao [b]

[a] Shaanxi Key Laboratory of Friction Welding Technologies, Northwestern Polytechnical University, No 127, West Youyi Road, Xi'an 710072, PR China
[b] Laboratoire d'Etudes et de Recherches sur les Matériaux, les procédés et les Surfaces(LERMPS), Université de Technologie de Belfort-Montbéliard, 90010 Belfort, France

HIGHLIGHTS

- Dense lanthanum silicate coatings were deposited by LPPS and VLPPS.
- Well-crystallized lanthanum silicate coating can be prepared by one-step VLPPS.
- The specific permeability of coating deposited by VLPPS is 1.79×10^{-19} m^2.

ARTICLE INFO

Article history:
Received 10 June 2012
Received in revised form
5 September 2012
Accepted 8 September 2012
Available online 20 September 2012

Keywords:
Lanthanum silicate
Low pressure plasma spraying
Very low pressure plasma spraying
Specific permeability
Solid oxide fuel cell

ABSTRACT

Magnesium doped lanthanum silicate with apatite-type structure, as a solid electrolyte for IT-SOFC (intermediate-temperature solid oxide fuel cells), was prepared by solid state sintering. The electrolyte coatings were fabricated by LPPS (Low Pressure Plasma Spraying) and VLPPS (Very Low Pressure Plasma Spraying). Their microstructures and phase composition were characterized by SEM and XRD. The gas permeability of coatings was measured with pure H_2 and O_2 at room temperature. It is shown that dense lanthanum silicate coatings can be obtained by LPPS and VLPPS. Amorphous and trace phases existed in coating deposited by LPPS. Well-crystallized lanthanum silicate coating can be prepared by one step VLPPS. The specific permeability of coating fabricated by VLPPS is 1.79×10^{-19} m^2.

1. Introduction

SOFCs (solid oxide fuel cells) are regarded as promising electrochemical devices which can directly convert chemical energy into electrical energy because of their high efficiency [1]. Each single cell mainly consists of three ceramic parts: anode, electrolyte and cathode. The electrolyte, separating anode and cathode, must be dense to prevent the mixing of combustible and oxygen. In addition, it must be a pure ionic conductor at its working temperature. The widely used yttria stabilized zirconia (YSZ) works as electrolyte on at high temperatures (900–1000 °C). These temperatures contribute dramatic drawback, such as thermal stress, high cost, etc. to overcome these disadvantages, other oxide ion conductors, working as electrolyte for IT-SOFC (intermediate temperatures solid oxide fuel cells) operating at 600–800 °C, are actively investigated. In these oxides, SiO_4 based apatite structural electrolyte materials, exhibits high ionic conductivity at lower temperatures and excellent chemical stability [2–5].

However, lanthanum silicate, as a new electrolyte, also raises the challenge in terms of phase stability and gas impermeability during the preparation of their electrolyte film. The conventional technologies, such as PVD (Physical vapour deposition), solid sintering, sol–gel and APS (Air plasma spraying), have been utilized [6–8]. Especially the last process has the potential of low cost production because of high deposition rates and the ability to coat large surface. However, it is difficult to fabricate dense and impermeable electrolyte layers by single APS process. Some post treatments, such as spark plasma sintering [9], high-temperature vacuum sintering [10], and chemical impregnation densification [11,12], can improve the electrolyte density and impermeability. In addition, the presence of amorphous phase in the plasma sprayed lanthanum silicate

* Corresponding author. Shaanxi Key Laboratory of Friction Welding Technologies, Northwestern Polytechnical University, No 127, West Youyi Road, Xi'an 710072, PR China. Tel./fax: +86 2988491426.
E-mail address: sunfu1981@hotmail.com (F. Sun).

0378-7753/$ – see front matter © 2012 Elsevier B.V. All rights reserved.
http://dx.doi.org/10.1016/j.jpowsour.2012.09.034

Table 1
Parameters of LPPS and VLPPS.

	VLPPS	LPPS
Pressure (mbar)	1	200
Courent (A)	700	700
Flow rate of Ar (slpm)	48	45
Flow rate of H_2 (slpm)	6	14
Distance (mm)	700	260
Torch	F4vb	F4vb
Substrate temperature (°C)	840	1050

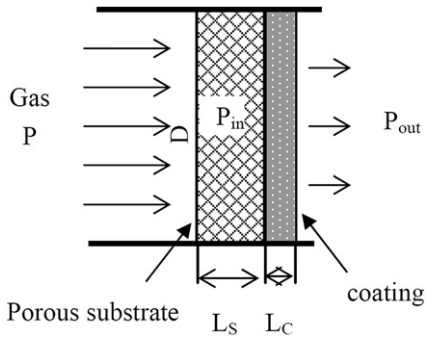

Fig. 1. Schematic of the measurement of permeability of the coating deposited on the porous substrate. k_s is the permeability of the porous substrate, 3.36×10^{-13} m^2, L_s is the thickness of the substrate; P is the pressure at the substrate side; P_{in} is the pressure of the interface between substrate and coating; A is the area of the sample, k_C is the permeability of the coating; L_C is the thickness of the coating; P_{out} is the pressure at outside of the coating.

coatings cannot be avoided, even if small powers were applied or the substrate was preheated. Therefore, heat treatment has been used to realize the recrystallisation.

Compared to APS, LPPS (Low Pressure Plasma Spraying) and VLPPS (Very Low Pressure Plasma Spraying) operate at lower pressures. Accordingly, these two plasma spraying processes facilitate to reduce the interaction of molten particles with surrounding cold gases and accelerate them to higher velocities [13–15]. The coatings produced by LPPS and VLPPS are denser than those produced by APS. In addition, preheating substrate without oxidation may be carried out by longer plasma jet.

The aim of this paper is to fabricate the dense and well-crystallized $La_{10}Si_{5.8}Mg_{0.2}O_{26.8}$ coatings. $La_{10}Si_{5.8}Mg_{0.2}O_{26.8}$ was prepared by traditional solid sintering. Its coatings were deposited by LPPS and VLPPS. The properties of coatings such as microstructure, phase composition and permeability were evaluated.

2. Experimental

Magnesium doped lanthanum silicates were prepared by traditional solid phase reactive sintering using high purity oxides: La_2O_3(99.99%), SiO_2(99.99%) and MgO(99%). Lanthanum oxide was pre-calcined at 1000 °C for 4 h in order to achieve dehydration before weighing. These three powders were mixed in stoichiometry composition of $La_{10}Mg_{0.2}Si_{5.8}O_{26.8}$, and the mixture was pressed into discs. Two-steps sintering were performed at 1400 °C for 10 h and 1600 °C for 15 h in air furnace. Between these two steps, the samples were ground and pressed again. Finally, the sintered samples were reground to powders and sieved as feedstock powders for plasma spraying. In order to reveal the microstructures of sintered samples, their surfaces were polished with a SiC paper and thermally etched at 1300 °C for 30 min.

A vacuum plasma spray system was employed to prepare $La_{10}Si_{5.8}Mg_{0.2}O_{26.8}$ coatings. Plasma spraying process was performed using a torch F4-VB (Sulwer Metco) with Ar primary plasma gas and powder carrier gas and H_2 secondary plasma gas. Two kinds of substrate were used to deposit the coatings: 3 mm thickness stainless steel plate and 2 mm thickness porous Ni/Al_2O_3 cermet produced by flame spraying. The former was applied to prepare the coating for microstructure and phase analysis, and the latter was used to prepare the coating for permeability measurement. Before coating deposition, the vacuum chamber was pumped down to the working pressure. The substrates were preheated using plasma jet, and their temperatures were detected by an infrared detector. The detailed parameters are listed in Table 1.

Phase compositions of characterization of sintered $La_{10}Si_{5.8}Mg_{0.2}O_{26.8}$ sample and its coatings were carried out by XRD (a Siemens D5000) using Co Kα radiation. Their microstructures were examined using a scanning electron microscopy (JSM5800LV JEOL, Japan). Based on cross-sectional BSE (Back-scattered electrons) images of the coatings, the porosity was evaluated by calculating the total area fraction of pores in the whole image using Scion image software. To estimate the porosity accurately, ten images in random areas were used for each kind of coating. The calculations were performed as following: firstly, BSE grey-scale images were converted to binary image by a thresholding process: solid parts were displayed in white and defects regions (i.e. pores and microcracks) in black. Secondly, a filter was applied performing an erosion operation, followed by dilation which smoothed objects and removed isolated pixels occupied by small-sized objects such as microcracks. Finally, residual black pixels occupied were counted and the total porosity was determined.

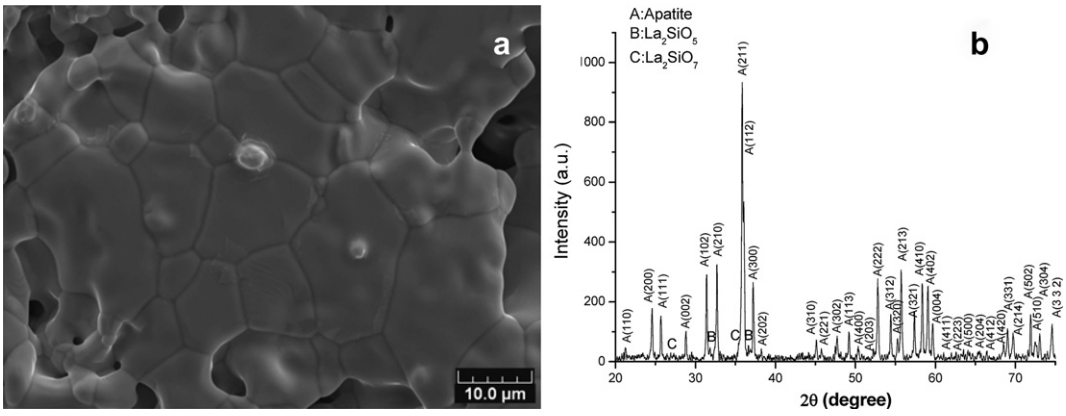

Fig. 2. $La_{10}Si_{5.8}Mg_{0.2}O_{26.8}$ pellets sintered at 1600 for 15 h: (a) SEM micrographs of the surface and (b) XRD patterns.

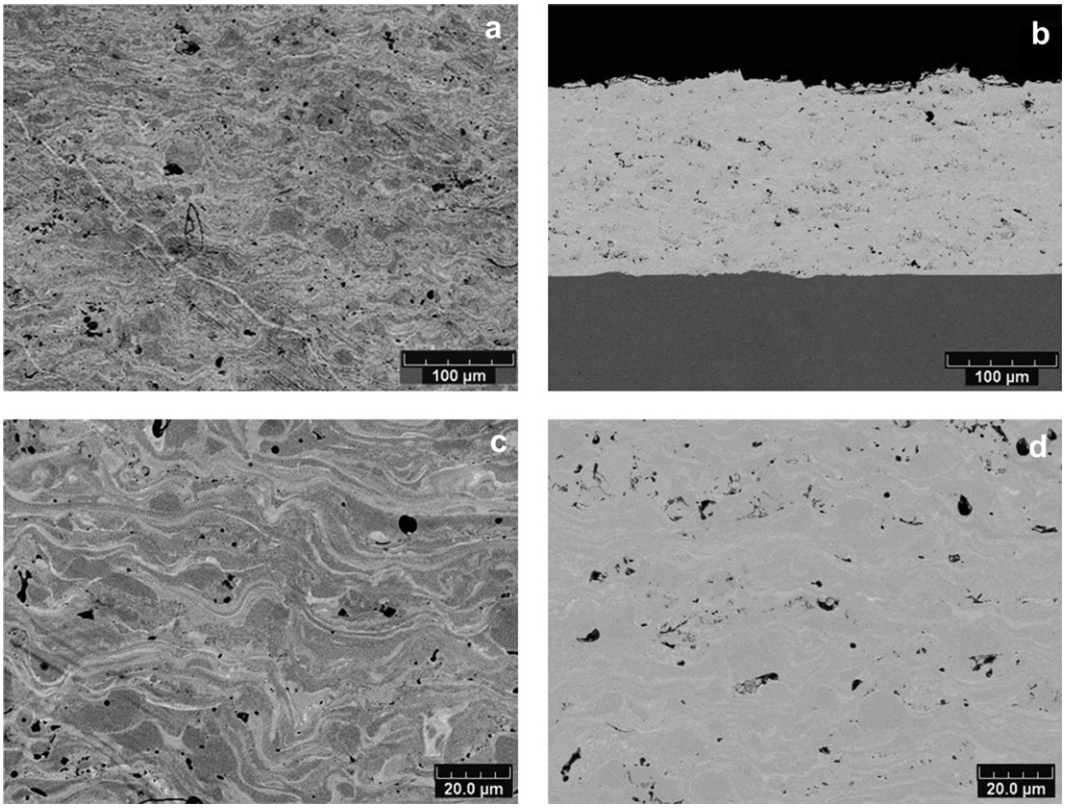

Fig. 3. SEM cross-section of $La_{10}Mg_{0.2}Si_{5.8}O_{26.8}$ coatings deposited by LPPS (a) (c) and VLPPS (b) (d).

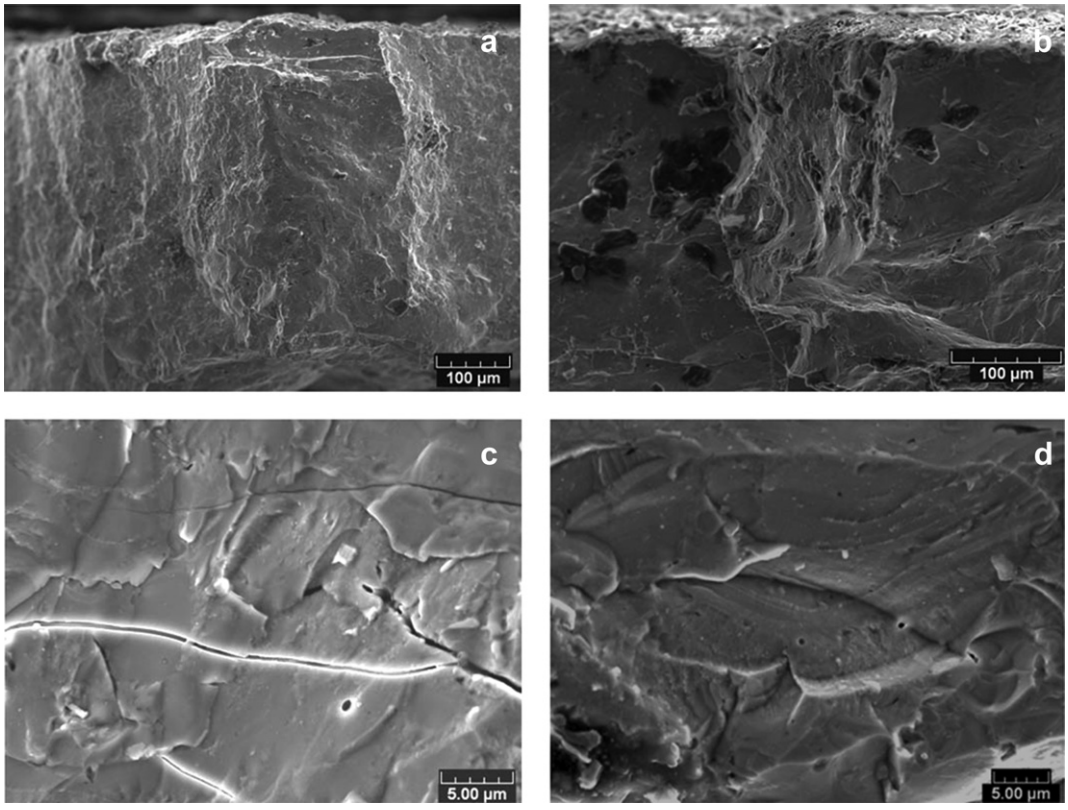

Fig. 4. SEM micrographs of fracture surface of $La_{10}Mg_{0.2}Si_{5.8}O_{26.8}$ coatings deposited by LPPS (a) (c) and VLPPS (b) (d).

Gas permeabilities of coatings deposited by VLPPS and porous Ni/Al_2O_3 cermet were measured at room temperature using the home-made equipment. Several pressure differences of gas (H_2 or O_2) were applied between two sides of the measured coating. Meanwhile, the flow rates of the gas were measured by a flow meter (Drycall Ml-500, USA) or water displacement method. The specific permeability can be determined by the Darcy's law:

$$k = \frac{Q \cdot \eta}{A \cdot \Delta P} \cdot \mu \quad (1)$$

where k is the specific permeability of the material (m^2); Q is the gas flow rate ($m^3\ s^{-1}$); A is the cross-sectional area of coating (m^2); η is the thickness of coating (m); ΔP is the pressure drop (Pa); μ is the dynamic viscosity of gas (Pa s). The specific permeability of porous Ni/Al_2O_3 cermet was calculated by the Equation (1). However, the specific permeability of the $La_{10}Si_{5.8}Mg_{0.2}O_{26.8}$ coating deposited on the porous substrate cannot be directly evaluated by the Equation (1). The Fig. 1 shows the schematic of the measurement of permeability of the coating deposited by VLPPS on the porous substrate. In order to precisely evaluate the specific permeability of the $La_{10}Si_{5.8}Mg_{0.2}O_{26.8}$ coating deposited on the porous substrate, the calculation is carried out by the following process: according to the Equation (1), the pressure difference between the two sides of the porous substrate can be calculated by the following equation

$$P - P_{in} = \frac{Q \cdot L_S}{k_S \cdot A} \cdot \mu \quad (2)$$

where, k_s is the specific permeability of the porous Ni/Al_2O_3 substrate, $3.36 \times 10^{-13}\ m^2$; L_s is the thickness of the substrate; P is the pressure at the substrate side; P_{in} is the pressure of the interface between substrate and coating; A is the area of the sample.

The pressure difference between both sides of the deposit can be calculated by the following equation:

$$P_{in} - P_{out} = \frac{q \cdot L_C}{k_C \cdot A} \cdot \mu \quad (3)$$

where, k_C is the permeability of the coating; L_C is the thickness of the coating; P_{out} is the pressure at outside of the coating.

According to Equations (2) and (3), the specific permeability of the coating can be calculated by:

$$k_C = \frac{q \cdot L_C}{A \cdot \left[P - P_{out} - \frac{q \cdot L_S}{K_S \cdot A} \cdot \mu \right]} \quad (4)$$

3. Results and discussion

3.1. Sintered $La_{10}Si_{5.8}Mg_{0.2}O_{26.8}$ sample

Fig. 2a presents the microstructure of $La_{10}Si_{5.8}Mg_{0.2}O_{26.8}$ sample sintered by two step sintering. Polycrystalline grains, grain boundaries and residual pores are showed. Medium Grains size is about 10 μm, which is caused by the high temperature (1600 °C) and the long period (15 h) of the treatment. In addition to grains and grain boundaries, there are still many residual pores, which can lead to a low density. However, these residual pores have no significant impact on plasma sprayed coating, because $La_{10}Si_{5.8}Mg_{0.2}O_{26.8}$ particles were melted and solidified during plasma spraying.

In Fig. 2b, the XRD pattern of sintered $La_{10}Si_{5.8}Mg_{0.2}O_{26.8}$ sample is showed. The apatite phase indexed with JCPDS 53-0219 is

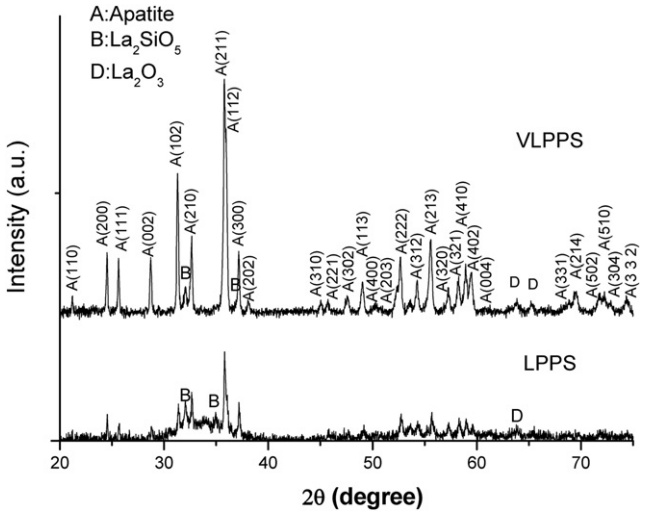

Fig. 5. XRD patterns of coatings deposited by LPPS and VLPPS.

presented. However, La_2SiO_5 and $La_2Si_2O_7$ as secondary phases exist in sintered sample. These two phases usually were observed during the preparation of lanthanum silicate by solid sintering, which is resulted from the imprecise stoichiometric reaction of La_2O_3 and SiO_2 powder during the preparation [16,17]. In this paper, the La_2O_3 pre-calcination was performed before weighing in order to achieve dehydratation. The possible reason is the inhomogeneous mixing of La_2O_3 and SiO_2 at local regions especially before the first step sintering.

3.2. Coatings microstructure

Fig. 3 shows the cross sectional microstructures of $La_{10}Si_{5.8}Mg_{0.2}O_{26.8}$ coatings deposited by LPPS and VLPPS on the stainless steel plate. The porosity of coatings deposited by VLPPS is $1.35 \pm 0.61\%$, which is similar to that of coatings deposited by LPPS (equal to $1.42 \pm 0.82\%$). These low porosities confirm that the particles are melted and spread out for the projection. Besides lower porosity, there are no visible cracks in the coatings produced by LPPS and VLPPS.

Fig. 4 presents the fracture surface morphology of the coatings prepared by LPPS and VLPPS. It is difficult to find unbonded

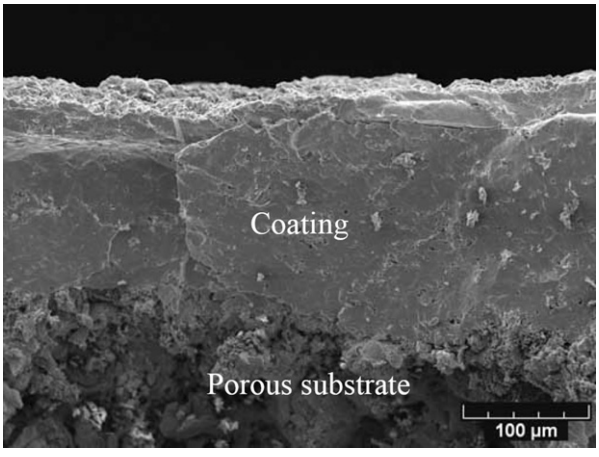

Fig. 6. Micrographs of fracture surface of the $La_{10}Si_{5.8}Mg_{0.2}O_{26.8}$ coating deposited by VLPPS on porous Ni/Al_2O_3 cermet for gas permeability measurement.

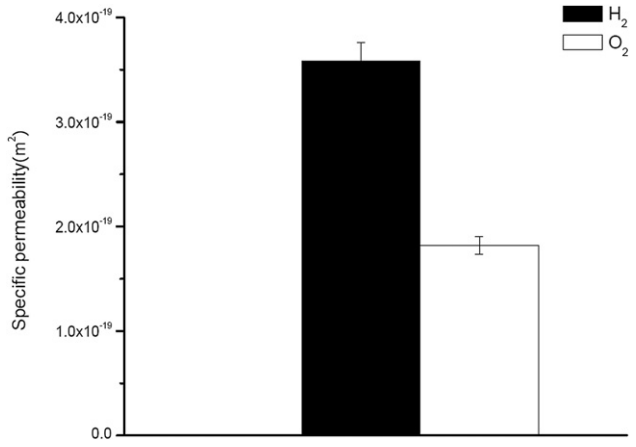

Fig. 7. Measured specific permeabilities of $La_{10}Mg_{0.2}Si_{5.8}O_{26.8}$ coatings deposited by VLPPS.

interfaces between the lamellas. Microcracks parallel to the substrate exist in the coating obtained by LPPS. It can be attributed to stress relaxation that is caused by the difference of thermal expansion coefficient between deposit and substrate.

It is noted that LPPS and VLPPS can ameliorate the microstructures of coatings compared to the APS, particularly the reduction of the porosity and microcracks. LPPS and VLPPS operate at lower pressure. The effect of pressure on temperature and particle velocity for plasma spraying, low pressure was studied in literature [18]. A low pressure facilitates to increase the speed of the plasma jet. After injection into the high velocity jet, the particles obtain a large kinetic energy and are therefore strongly accelerated. This increase the impact force of melted particles, and thus promotes the adhesion of particles. In addition, the plasma jet at lower pressure is longer and of larger diameter which facilitates the preheating of the substrate and reduces its oxidation. Increasing the substrate temperature can improve the connection between slices. On the contrary, the temperature of the particles decreases as a function of the operating pressure. However, the relatively low melting temperature of lanthanum silicate, facilitates its melting in the plasma jet at very low pressure. The microstructure of the deposits prepared by VLPPS shows that the particles are melted during the spraying. In addition, the preheating temperature of the substrate during the projection VLPPS is higher than that of the projection LPPS. This helps explain the improvement of microstructures prepared by deposition VLPPS compared to that obtained by LPPS.

3.3. Phase composition

Fig. 5 shows the XRD patterns of $La_{10}Si_{5.8}Mg_{0.2}O_{26.8}$ coatings fabricated by LPPS and VLPPS. In the coating deposited by LPPS, a majority of peaks corresponds to standard $La_{10}Si_6O_{27}$ (JCPDS 53-0219). A broad bump indicates the presence of the amorphous phase in the coating. In addition to apatite and amorphous, traces phase La_2SiO_5 and La_2O_3 exists in the coating. This confirms that the projection LPPS cannot eliminate the amorphous phase in the coating.

In the coating prepared by VLPPS, it remains the crystal structure of apatite despite the presences of the secondary phases La_2SiO_5 and La_2O_3. Generally, the formation of the amorphous phase is caused by the high cooling rate. Longer plasma jet of VLPPS facilitates to heat the substrate. Thus, a higher substrate temperature 1050 °C was realized in this study. In addition, the cooling rate of the coating after the projection decreases with decreasing the working pressure due to the reduction in heat loss caused by convection. Therefore, VLLPS is a good method for inhibiting the formation of amorphous phase in $La_{10}Si_{5.8}Mg_{0.2}O_{26.8}$ coatings due to a higher substrate temperature and lower cooling rate of the coating.

3.4. Permeability

Fig. 6 presents the micrographs of fracture surface of the $La_{10}Si_{5.8}Mg_{0.2}O_{26.8}$ coating deposited by VLPPS for gas permeability measurement. The coating with about 100 microns thickness was prepared on the porous Ni/Al_2O_3 cermet.

Fig. 7 shows the specific permeability of the deposit prepared by VLPPS. The measured value with hydrogen (3.58×10^{-19} m^2) is higher than that measured with oxygen (1.79×10^{-19} m^2). The specific permeability is the parameter which measures the contribution of the porous medium to the conductivity, and its value depends uniquely on pores geometry [19]. The dynamic viscosity describes a fluid's internal resistance to flow and may be thought of as a measure of fluid friction. Generally, dynamic viscosity of the gas is the function of temperature and pressure [20]. However, in the micro or nanochannel, the gas viscosity is less than that at the macroscale because collisions between gas molecules are less frequent in high Knudsen number flows and there are more collisions with the wall [21]. In this study, dynamic viscosity as the function of temperature and pressure was used to calculate the specific permeability. It resulted in the difference between specific permeabilities measured with H_2 and O_2.

The specific permeability of the coating obtained by VLPPS is lower than the coating produced by APS (10^{-15}–10^{-16} m^2) [22]. In the coating deposited by plasma spraying, the gas can pass the coating through the path consisted by open pores and microcracks

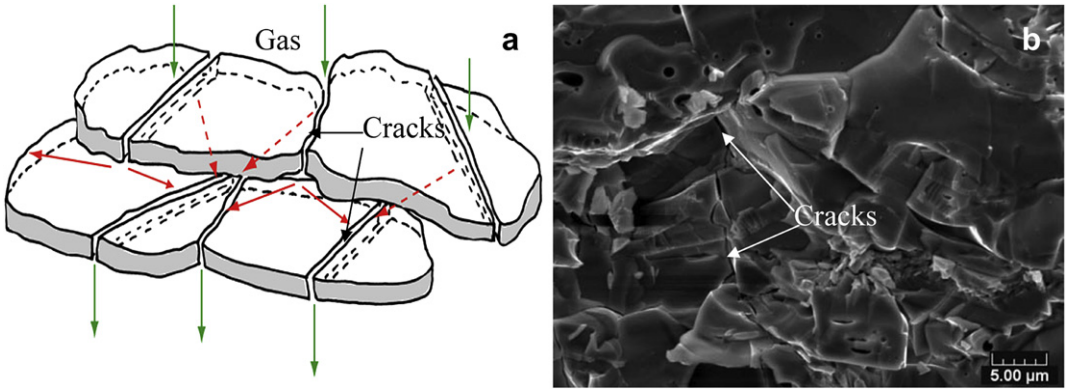

Fig. 8. Geometrical representation of gas flow paths in plasma sprayed coating (a) [23] and micrographs of fracture surface of the $La_{10}Si_{5.8}Mg_{0.2}O_{26.8}$ coating deposited by APS (b) [22].

as shown in Fig. 8a [23]. The porosity in coating prepared by VLPPS is lower than that in coating deposited by by APS (3.12%) [22]. A low porosity of the as-sprayed coating causes low gas permeability [24]. In addition, the microcracks can be found in fracture surface of coating deposited by APS, as shown in Fig. 8b. In contrast, the microcracks cannot be easily found in fracture surface of coating deposited by VLPPS, as shown in Fig. 4b and d. Therefore, the coating prepared by VLPPS has low porosity and no obvious cracks. Accordingly, the decreasing of gas flow channels in the coating deposited by VLPPS contributes low specific gas permeability compared with that fabricated by APS.

It has been pointed out that the gas permeability required for electrolyte layer in the application to SOFCs is less than 1.0×10^{-6} cm^4 gf^{-1} s^{-1} [25]. By converting the unit to international system of units, the corresponding value is 1.02×10^{-12} m^2 Pa^{-1} s^{-1}. Obviously, the impermeability of the lanthanum silicate coatings deposited by VLPPS can meet the requirement as the electrolyte for SOFC.

4. Conclusions

In this study, LPPS and VLPPS were used to prepare $La_{10}Si_{5.8}Mg_{0.2}O_{26.8}$ coating as electrolyte for IT-SOFC. Both processes could deposit dense coatings. In addition to the phase of apatite, amorphous phases and secondary phases La_2SiO_5 and La_2O_3 were detected in the coatings obtained by LPPS. However, in the coating produced by VLPPS, the crystal structure of apatite was preserved after the projection, despite the presence of the secondary phase La_2SiO_5 and La_2O_3. In addition, the coating prepared by one-step VLPPS, has a relatively low specific gas permeability (1.79×10^{-19} m^2).

References

[1] N.Q. Minh, Solid State Ionics 174 (2004) 271–277.
[2] P.R. Slater, J.E.H. Sansom, J.R. Tolchard, The Chemical Record 4 (2004) 373–384.
[3] T. Nakao, A. Mineshige, M. Kobune, T. Yazawa, H. Yoshioka, Solid State Ionics 179 (2008) 1567–1569.
[4] H. Yoshioka, S. Tanase, Solid State Ionics 176 (2005) 2395–2398.
[5] H. Yoshioka, Journal of Alloys and Compounds 408–412 (2006) 649–652.
[6] H. Yoshioka, T. Mitsui, A. Mineshige, T. Yazawa, Solid State Ionics 181 (2010) 1702–1712.
[7] S. Dru, E. Meillot, K. Wittmann-Teneze, R. Benoit, M.L. Saboungi, Surface and Coatings Technology 205 (2010) 1060–1064.
[8] W.Z. Wang, F. Sun, X.P. Guo, H.L. Liao, Surface and Coatings Technology 205 (2011) 3665–3670.
[9] K.A. Khor, L.G. Yu, S.H. Chan, X.J. Chen, Journal of the European Ceramic Society 23 (2003) 1855–1863.
[10] M. Scagliotti, F. Parmigiani, G. Samoggia, G. Lanzi, D. Richon, Journal of Materials Science 33 (1988) 3764–3770.
[11] L. Rose, O. Kesler, Z. Tang, A. Burgess, Journal of Power Sources 167 (2007) 340–348.
[12] C.J. Li, C.X. Li, X.J. Ning, Vacuum 73 (2004) 699–703.
[13] Z. Salhi, D. Klein, P. Gougeon, C. Coddet, Vacuum 77 (2005) 145–150.
[14] H. Hamatani, W.S. Crawford, M.A. Cappelli, Surface and Coatings Technology 162 (2002) 79–92.
[15] K.H. Baik, P.S. Grant, B. Cantor, Acta Materialia 52 (2004) 199–208.
[16] E. Béchade, I. Julien, T. Iwata, O. Masson, P. Thomas, E. Champion, K. Fukuda, Journal of the European Ceramic Society 28 (2008) 2717–2724.
[17] Y.L. Kuo, Y. Y Liang, Ceramics International 38 (2012) 3955–3961.
[18] Z Salhi, Développement de techniques pour le diagnostic des procédés de projection thermique sous pression réduite, Thesis Université de Technologie de Belfort-Monbéliard, 2004.
[19] S.J. Lukasiewicz, J.S. Reed, Journal of the American Ceramic Society 71 (1988) 1008–1014.
[20] J.O. Hirschfelder, C.F. Curtiss, R.B. Bird, Molecular Theory of Gases and Liquids, Wiley, New York, 1954.
[21] Q.X. Liu, P.X. Jiang, H. Xiang, Chinese Science Bulletin 57 (2013) 1488–1493.
[22] F. Sun, H. Liao, N. Zhang, O. Rapaud, C. Coddet, Plasma Sprayed Electrolyte of Magnesium Doped Lanthanum Silicate with Apatite-Type Structure, International Thermal Spray Conference & Exposition 2010 (2010) 880–883.
[23] I.O. Golosnoy, S. Paul, T.W. Clyne, Acta Materialia 56 (2008) 874–883.
[24] H. Tsukuda, A. Notomi, N. Hisatome, Journal of Thermal Spray Technology 9 (2000) 364.
[25] C.J. Li, C.X. Li, Y.Z. Xing, M. Gao, G.J. Yang, Solid State Ionics 117 (2006) 2065–2069.